Structure and magnetic properties of MnN, CrN, and VN under volume expansion

M. S. Miao and Walter R. L. Lambrecht
Department of Physics, Case Western Reserve University, Cleveland, Ohio 44106-7079, USA
(Received 6 July 2004; revised manuscript received 17 December 2004; published 3 June 2005)

Using a first principles density functional method, we studied how the structure and the magnetic properties of the early transition metal nitrides MnN, CrN, and VN change with expansion and compression of volume. We found that the zinc blende (ZB) state is lower in energy for MnN than the experimentally observed slightly tetragonally distorted θ phase, which suggests that the latter is stabilized by N vacancies. Under small volume compression the rock salt (RS) structure becomes lower in energy than the ZB one. While at its theoretical equilibrium lattice constant MnN is found to have ferromagnetic (FM) order, it becomes antiferromagnetic AFM-$[001]_1$ ordered for larger lattice constants in agreement with experiment. The ZB phase is nonmagnetic for its minimum energy lattice constant and below but develops first AFM[001] order and then AFM$[111]_1$ order for larger lattice constants. For CrN and VN, the global energy minimum corresponds to the RS structure. Under a certain volume expansion, both NiAs and ZB structures can become metastable. CrN exhibits antiferromagnetic order in the NiAs structure ($[0001]_1$) and the RS phase ($[110]_1$) and ferromagnetic order in the ZB structure. Under lattice expansion the RS structure magnetic configuration changes from $[110]_1$ to $[110]_2$, the experimentally observed structure at equilibrium when an orthorhombic distortion is taken into account, and finally to FM at even larger lattice constant. VN has nonzero magnetic moment at a volume around or larger than the equilibrium volume. However, its magnetic interactions among the neighboring moments are very weak as the energy differences between the FM and the AFM ordering are very small. The ferromagnetic states of all three nitrides in the ZB structure become half-metallic under large volume expansion. The partial densities of states (PDOS) for each sublattice in the AFM states show similar structure to the PDOS in the FM state. The effects of the volume expansion on the electronic structure of ZB and RS structure are discussed in detail.

DOI: 10.1103/PhysRevB.71.214405 PACS number(s): 75.50.Ee, 75.30.Et, 71.20.Ps

I. INTRODUCTION

The recent interest in spintronics not only inspired the intensive search for new magnetic semiconductor materials such as the transition metal doped III-V compounds but has also revived an interest in new metallic magnetic compound materials. The transition metal nitrides, especially CrN[1–5] and MnN[6–9] have been studied intensively in past years. In contrast to previous studies that mainly concentrated on the bulk properties of the compounds, recent research for spintronic materials has focused on thin films and nanosize particles grown on semiconductor substrates and on high concentration doping in suitable semiconductors in which the transition metal nitride clusters may form by precipitation. One common distinct feature of these systems is that the transition metal compound volume can be very different from its bulk equilibrium value. This is the result of the large strain imposed by the substrate or the host. Therefore, the studies of the volume dependence of the structure, the electronic and the magnetic properties of these transition metal nitrides is important for understanding the properties of these compounds in film or small clusters form.

Recently, the successful growth of thin film or nanosize particles of Cr and Mn pnictides, such as CrAs,[10] CrSb,[11] and MnSb,[12] on the surface of III-V semiconductors inspired many experimental and theoretical studies of these compounds under volume expansion.[13–24] It was found that although most of these compounds are stable in sixfold coordinated NiAs or MnP structures in the bulk, they do form simple fourfold coordinated zinc blende (ZB) structures in the films or nanoparticles. Several calculations showed that the ZB structure is metastable for these compounds under volume expansion. The major reason that these compounds attracted so much attention is that they can exhibit the half-metallic state in the ZB structure and under volume expansion. This shows that half-metallicity[25–28] can exist in a simple structure. It is usually believed that the half-metallicity can only exist in more complex structures. Recent theoretical calculations showed that the half-metallicity is mainly the result of local bonding and also occurs in wurtzite (WZ) and other tetrahedrally coordinated polytypes.[24,29] This is why Mn-doped GaAs was also found to be half-metallic. It is important to study the same situation for nitrides, especially considering that Cr- and Mn-doped GaN have been claimed to be room-temperature ferromagnetic semiconductors.[30,31] Although this has also been predicted by theory,[32] and the formation of magnetic moments and ferromagnetic exchange coupling between near neighbors was also confirmed by first-principles calculations,[33] there is still a lot of controversy over the question whether this observed room-temperature ferromagnetic behavior is truly carrier-mediated or due to unidentified secondary phases.[34–37] Such secondary phases could occur in nanosize particle form and thereby be difficult to detect with standard analytical techniques.

In this paper, we systematically studied the structure and magnetic properties of three transition metal nitrides, VN, CrN, and MnN, under volume expansion and compression. Four different structures, including NiAs, NaCl, ZB, and WZ are considered. Both magnetic and antiferromagnetic states

are calculated for each compound in all four structures. In Sec. II, we briefly introduce the computational method employed in this paper. Section III, describing our main results is organized as follows. First we describe the total energy and structural preference results in Sec. III A, next we discuss the electronic structure and magnetism in Sec. III B and finally we discuss the half-metallic state under large volume compression in Sec. III C. Finally, we summarize the conclusions of the paper in Sec. IV.

II. COMPUTATIONAL METHODS

Our calculations are based on the density functional theory.[38,39] The von Barth and Hedin spin polarized exchange and correlation potential[40] is used in the local spin density functional approximation. A full potential linear muffin-tin orbital (LMTO) method[41] was employed. Important features of this method are (1) it treats the smooth part of the charge density in the interstitial region accurately and efficiently by means of a real space mesh throughout the cell and using fast Fourier transforms, (2) it uses an efficient minimal basis set of augmented smoothed Hankel functions,[42] and (3) it uses a force theorem to calculate forces analytically and has a capability to relax structures by means of a conjugate gradient method. Augmentation means that inside the muffin-tin spheres, whose radii are chosen to be nearly touching, the envelope function is replaced by a matching linear combination of spherical harmonics Y_{lm} times the solutions $\phi_{l\nu}$ of the radial Schrödinger equation of the spherical part of the potential at that site and their energy derivatives $\dot{\phi}_{l\nu}$ at a chosen linearization energy $E_{l\nu}$, chosen to be in the center of gravity of each occupied partial density of states $N_l(E)$. The convergence parameters of the calculation include the number of points in the real space mesh, the number of basis functions and their chosen smoothing radii, which determines the behavior of the basis function just outside the muffin-tin radius and $\kappa^2 = E - V_{mtz}$ value which determine the long-range decay of the envelope function, and the number of **k** points in the Brillouin zone integration. For high accuracy, we adopt two sets of basis functions for the *s*, *p*, and *d* orbitals of the transition metal atoms and the *s* and *p* orbitals of the group V atoms. Only one basis function is used for the group V *d* orbital. The smoothing radii and κ values of the two basis functions are chosen to be rather different so as to give more variational freedom to the basis set and are optimized in some initial test calculations to minimize the total energy.

The four structures studied in this paper are either fourfold or sixfold coordinated. The energy difference between the two structures with the same coordination is usually small. Compared to semiconductors, the calculation for metallic systems usually needs a larger **k** mesh because the Fermi surface may have a complex shape. We calculate all the structures in a hexagonally shaped unit cell. These cells are supercells containing three close-packed fcc layers of cation and anion (i.e., three formula units) rather than the primitive unit cells for the cubic structures and have of course only trigonal, not hexagonal symmetry when taking into account the atomic filling of the cell. For the hexagonal structures, they are primitive cells and contain two formula units. The important point is that this choice of cells allows us to use an exactly equivalent set of **k** points for the hexagonal and cubic phases by dividing the BZ in the **c** direction in a number of points in the ratio 2:3 for cubic to hexagonal phases. In the plane perpendicular to the **c** direction, we choose the same number of divisions. It is expected that in this procedure the small numerical errors arsing from slightly incomplete BZ sampling will cancel to a large degree. A similar procedure was shown in Ref. 43 to resolve the energy difference between SiC polytypes down to few tenths of 1 meV.

III. RESULTS

A. Total energy

Figures 1(a)–1(c) depict the total energy of MnN, CrN, and VN in all four structures for both FM and AFM states. The lattice constants shown in the figure are corresponding cubic lattice constants. Their relation to the hexagonal one is $a_{hex} = a_{cub}/\sqrt{2}$. The c/a ratios for NiAs structure are only optimized at the minimum point and are fixed for the other lattice constants. The optimized c/a ratios for NiAs structure are 1.64 for VN, 1.59 for CrN, and 1.59 for MnN. These values are quite close to the ideal value of 1.63. The c/a ratios for WZ structure are kept ideal for all compounds. Although various AFM orderings are considered, only one is shown here. The energy differences between different magnetic configurations is shown separately. We also calculated these structures without spin polarization. These calculations not shown, give similar conclusions about the structural preference but are slightly higher in energy.

The global energy minimum for MnN is found to correspond to the ZB structure. Only under about 4% of compression, the NaCl structure becomes lower in energy than ZB. This result is confirmed by our other calculations using Ceplay-Alder LDA and Perdew-Wang 91 GGA exchange correlation functionals. The GGA is only implemented in the atomic spherical approximated (ASA) LMTO code. However, for calculating the total energy for high symmetric structures, such as RS and ZB, ASA was proved to be sufficient. Although the energy differences between the minimum points for RS and ZB are slightly different for different calculations, they all show that ZB structure is globally stable. This is a surprising result because no ZB phase has been detected experimentally for MnN. At concentrations x close to 1 MnN_x is known to have a slightly tetragonally distorted rocksalt (RS) structure, known as the θ phase. The tetragonal distortion arises from the AFM-I ordering, in which spins are parallel within [001] planes but alter direction from one plane to the next.[8] It is not entirely clear however, that an exactly stoichiometric MnN compound has ever been synthesized. Most samples have a sizable concentration of N vacancies.[6,7] We speculate that this would reduce the lattice constant and thereby stabilize the RS structure. This effect could more carefully be tested by calculating the energy of formation of vacancies in RS and ZB. If the energy of formation is lower in RS than in ZB than the RS structure will become the preferred structure at some concentration of va-

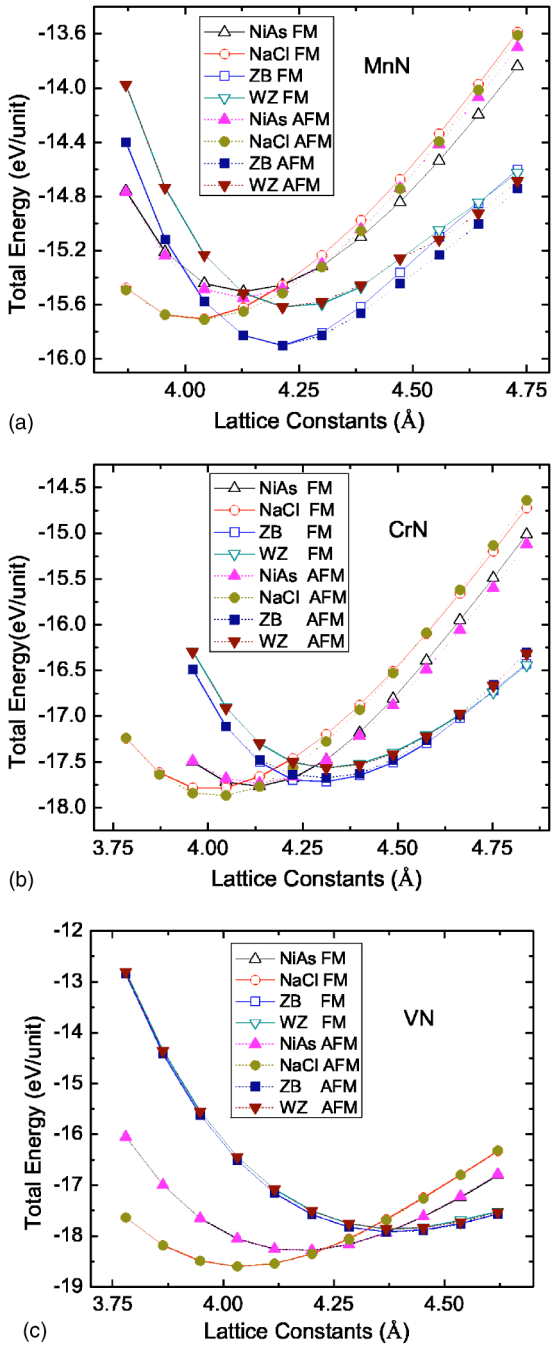

FIG. 1. (Color online) Total energy vs lattice constant for MnN (top), CrN (middle), and VN (bottom) in ZB, WZ, NaCl, and NiAs structures and for AFM (filled symbols) and FM (open symbols) ordering. The lattice constants are for cubic structure.

cancies. Calculations to test this are in progress but are outside of the scope of the present paper. The WZ phase is found to lie significantly higher in energy than the ZB phase. The NiAs phase has an equilibrium lattice constant in between those of ZB and RS but its energy is significantly higher than that of RS. So, under pressure we expect the transition to take place directly from ZB to RS without an intermediate NiAs phase.

Considering now the magnetic configurations, Fig. 1 indicates that both the RS and ZB phases prefer AFM over FM ordering over the range of lattice constants where the two curves are distinguishable. Closer inspection however reveals that at the minimum energy lattice constant of RS and for lower lattice constants, the FM state has lower energy but the energy difference is essentially within the error bar of our calculations. For larger lattice constants, MnN prefers the AFM-AFM-$[001]_1$ ordering in agreement with experimental data for the θ phase. In ZB, the magnetic moment is zero for small lattice constants and up to about the minimum energy lattice constant. However, at larger lattice constants AFM-$[111]_1$ is the preferred state.

The minimum energy lattice constants, magnetic moments and cohesive energies for the different magnetic configurations and crystal structures at their respective minimum lattice constants are given in Table I together with the results for CrN and VN. The cohesive energy is defined as the absolute value of the binding energy that is the total energy shown in Fig. 1. This energy is calculated by subtracting the

TABLE I. Lattice constant, magnetic moment, and cohesive energy at the minimum energy of various phases of MnN, CrN, and VN.

	Structure	Magnetic order	a (Å)	μ	E (eV)
MnN	NaCl	FM	4.02	2.48	15.710
		AFM-$[001]_1$	4.02	2.40	15.689
		AFM-$[111]_1$	4.02	1.77	15.583
		AFM-$[110]_1$	4.02	2.41	15.692
		AFM-$[110]_2$	4.02	1.91	15.617
	ZB	non-FM	4.22	0	15.901
	NiAs	FM	4.13	1.52	15.504
		AFM[0001]	4.13	1.42	15.553
	WZ	FM	4.24	0.65	15.621
		AFM[0001]	4.24	0.03	15.627
CrN	NaCl	FM	4.0	1.40	17.801
		AFM-$[001]_1$	4.0	1.71	17.865
		AFM-$[111]_1$	4.0	1.84	17.801
		AFM-$[110]_1$	4.0	1.77	17.870
		AFM-$[110]_2$	4.0	1.80	17.826
	ZB	FM	4.3	1.44	17.731
		AFM-$[001]_1$	4.3	1.23	17.712
		AFM-$[111]_1$	4.3	1.16	17.687
	NiAs	FM	4.14	1.53	17.767
		AFM[0001]	4.14	1.50	17.736
	WZ	FM	4.31	1.34	17.568
		AFM[0001]	4.31	1.27	17.568
VN	NaCl	FM	4.03	0.19	18.598
		AFM[001]	4.03	0.18	18.598
	ZB	FM	4.41	0.65	17.878
		AFM[111]	4.41	0.43	17.892
	NiAs	FM	4.20	0.05	18.283
		AFM[0001]	4.20	0.01	18.283
	WZ	FM	4.41	0.27	17.832
		AFM[0001]	4.41	0.42	17.837

energies of each atom in spin polarized configuration from the total Kohn-Sham energy.

The preferred spin ordering directions are different for different structures. In the NaCl structures, the spin ordering is along the [001] direction, so-called AFM-I ordering, whereas in the ZB structure, it is along the [001] direction around the equilibrium volume but along the [111] direction (AFM-II) under large volume expansion ($a > 4.5$ Å). The spin ordering in NiAs and WZ structure is along the equivalent [0001] direction, i.e., perpendicular to their basal planes. Also in these phases we find that the AFM ordering is preferred over FM ordering for the equilibrium lattice constant and above. The ordering of different magnetic configurations and an analysis of the exchange parameters of RS MnN were presented previously in Ref. 8.

For CrN, the NaCl structure has the global energy minimum. It is 0.15 eV lower in energy than the metastable ZB structure, which has a minimum at a larger lattice constant. This energy difference is smaller than the analogous values for all the other transition metal pnictides and chalcogenides.[29] The NiAs structure again lies in between the ZB and RS and now the WZ structure is closer in energy to the ZB.

The NaCl structure is AFM at the equilibrium volume. The AFM-I state is lower in energy than the FM state by about 80 meV. Under volume expansion, this energy difference becomes smaller and smaller. At about 10% lattice constant expansion, the ferromagnetic state becomes stable. At about 4% lattice expansion, the ZB structure becomes metastable. Interestingly, at the lattice expansion of 2–4 %, the NiAs structure has the lowest energy. In this lattice constant range, it is ferromagnetic. The energy difference between the minima of the AFM NaCl and the FM NiAs structures is only 0.1 eV. The ZB structure is seen to prefer the FM state for all lattice constants. Under very large lattice expansion, the ferromagnetic WZ structure can become the one with lowest total energy.

Experiments[1,2,4,44] and previous calculations[5,45–48] found that the AFM ordering of CrN in NaCl structure was along the [110] direction. This AFM structure consists of (110) FM layers and its spin direction alternates after every two layers and can be labeled as $[110]_2$. This unusual AFM ordering is accompanied by a shear strain in the (001) plane that distorts the structure from cubic to orthorhombic. The AFM order built up also from (110) FM layers but with spin directions alternating every single layer is equivalent to the AFM [001] order. Therefore we can also label it AFM $[110]_1$. It was studied in a previous theoretical work and was found to be the most stable one at the equilibrium lattice constants but without structural distortion. To compare our calculations with the previous results and also to study the volume expansion effects on the complex magnetic ordering for CrN in NaCl structure, we calculated the FM, AFM-$[001]_1$, AFM-$[111]_1$, AFM-$[110]_1$, and AFM-$[110]_2$ orderings for CrN in NaCl. For each ordering vector, we calculate the energy difference from the FM ordering in compatible unit cells and with compatible **k**-point meshes. We present our results in Fig. 2. We found that the minima of the different AFM states occur at about the same lattice constant, 4.02 Å, which is very close to the FM equilibrium lattice constant. However, the energy difference from the FM case is maximum at a slightly larger lattice constant, as can be seen from the location of the minima in Fig. 2. Figure 2 shows that the AFM-$[110]_1$ state is the most stable one at the equilibrium volume. At the equilibrium volume, the FM state is higher in energy than the AFM-$[110]_1$ state by 72 meV, while the AFM-$[110]_2$ state lies only 44 meV above the ground state. These results are in good agreement with previous work. Filipetti *et al.*[5] find 75 and 34 meV for these energy differences respectively. In a Heisenberg model with only first and second nearest interactions the $[001]_1$ configuration (equivalent to the $[110]_1$) has the energy $2J_1 - 3J_2$. The FM configuration in this model has energy $-6J_1 - 3J_2$ while the $[111]_1$ configuration has energy $3J_2$ and the $[110]_2$ configuration has energy J_2. Interestingly, we find that under volume expansion, the AFM-$[110]_2$ state can become energetically favored even without the orthorhombic distortion. Under very large volume expansion, with lattice constants larger than 4.7 Å, the FM state becomes the lowest in energy. For MnN the results are totally different. The AFM-[001] order, or equivalently the AFM-$[110]_1$ order is always lowest in energy. The AFM-$[110]_2$ order is not close in energy to AFM-$[110]_1$ state and is higher in energy even than the FM state.

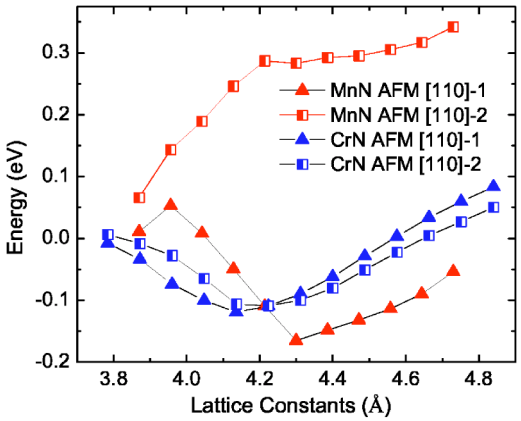

FIG. 2. (Color online) Energies of different AFM ordering for MnN and CrN in NaCl structure under different lattice constants. The energies are relative to the energy of the FM state.

These results can be understood by considering the types of exchange interactions. In CrN, the nearest neighbor interaction is antiferromagnetic and mainly due to direct exchange between t_{2g} orbitals. There is a weak ferromagnetic double exchange via e_g orbitals and N p orbitals.[48] The nearest neighbor exchange $J_1 \approx -9.5$ meV given by Filipetti *et al.*[5] is in fact very close to that in MnN, where Lambrecht *et al.*[8] give $J_1 \approx -9$ meV. On the other hand the second nearest neighbor interactions J_2 differ substantially. It is only 4 meV in CrN and 34 meV in MnN. This interaction arises from double exhange via N p orbitals between e_g orbitals. The lower filling of the d bands in Cr than in Mn means that fewer unpaired e_g electrons contribute to the magnetic moment, which reduces their interaction. Under volume expansion, one expects the direct antiferromagnetic exchange to become weaker and eventually become ferromagnetic because the overlap between Cr d orbitals decreases. This fol-

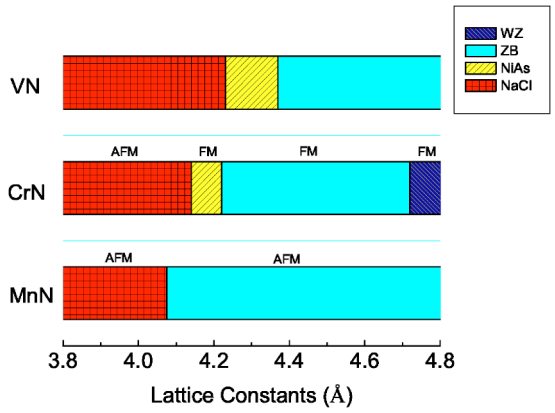

FIG. 3. (Color online) The stable and metastable structures and the magnetic ordering for different lattice constants.

lows for instance from the Heitler-London picture. On the other hand, we see that under compression, the FM state also becomes favored. This is probably because then the atomic-like localized picture starts to fail more and more and instead an itinerant theory like the Stoner theory is required.

For VN, the stability of the NaCl structure is much stronger: the minimum energy of NaCl is 0.68 eV lower than that of the ZB structure and is 0.31 eV lower than that of the NiAs structure. The WZ and ZB structures are now very close in energy, similar to what was encountered in other pnictides. On the other hand, the energy difference between the FM and AFM states are much smaller for all the structures in comparison with MnN and CrN, indicating that the magnetic interactions are much weaker for VN. Its magnetic moments are very small around the equilibrium volumes for both NaCl and ZB structures. But under volume expansion its magnetic moments increase significantly for both structures. Similar to CrN, there is also a range of lattice expansion in which the NiAs structure is metastable.

To finish this section, we summarize the results for the equilibrium phase and magnetic configuration as function of lattice constant in a phase diagram given in Fig. 3.

B. Electronic structure and magnetism

For the three nitrides studied in this paper, the NaCl structure is stable at smaller volume whereas the ZB structure is stable at larger volume. The energy of the WZ structure is usually slightly higher than that of the ZB structure. Because of the importance of the NaCl and the ZB structure, we will study their band structure and magnetism in more detail in this subsection.

Although the magnetic ordering is totally different for the FM and AFM states, their electronic structures are rather similar. We first study the FM configurations. Figure 4 presents the partial density of states (PDOS) for MnN in both NaCl and ZB structures and with both lattice constants of 4.3 and 4.9 Å. 4.3 Å is a value close to the calculated equilibrium lattice constants of ZB MnN, CrN, and VN. 4.9 Å is a value close to the lattice constants of InN, the nitride semiconductor with largest lattice constant. All the DOS show both the spin splitting and the crystal field splitting. In both structures, the d orbitals split into two groups as the spherical symmetry is reduced. In the NaCl structure, the e_g states ($d_{x^2-y^2}$ and $d_{3z^2-r^2}$) strongly couple with the nitrogen p and s states and form σ bonding and antibonding states with them. The t_{2g} states (d_{xy}, d_{yz}, and d_{zx}) only form weak π bonds with N p and do not interact with the N s orbitals. We may consider them as nonbonding to first approximation. Note that here we call these d orbitals t_{2g} and e_g according to the irreducible representations of the octahedral group O_h. The label g refers to the fact that they are even with respect to inversion. In the ZB case, these same sets of orbitals are labeled t_2 and e according to the tetrahedral group T_d which has no inversion and thus the subscript g is dropped. Now, the t_2 states are forming bonding and antibonding states with the nitrogen sp^3 hybrids which have however a mixed σ and π bonding character and would thus be expected to be somewhat weaker. From the four nearest-neighbor dangling bonds pointing directly toward the transition metal atom one can make three degenerate linear combinations with t_2 symmetry and a linear combination with a_1 symmetry. The latter does not interact with the e orbitals which are therefore essentially

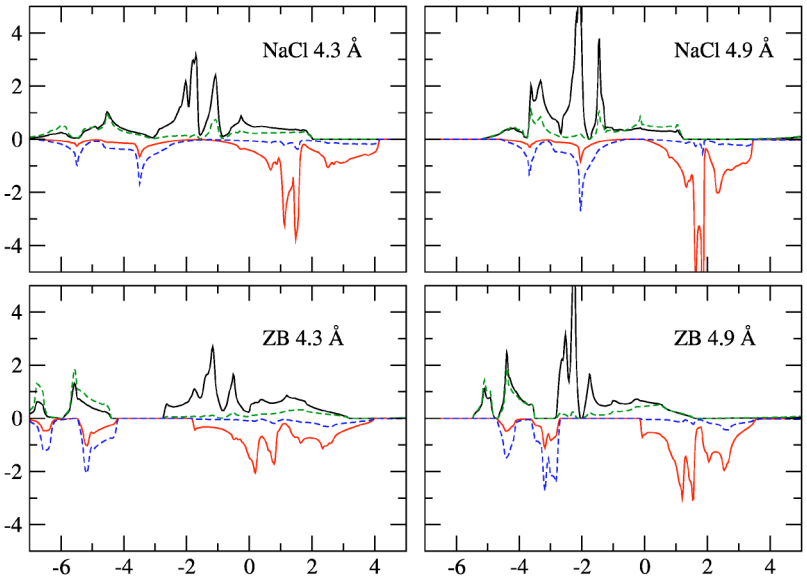

FIG. 4. (Color online) The PDOS for MnN in both RS and ZB structures and with lattice constants of 4.3 and 4.9 Å, respectively. Solid lines Mn d; dashed lines N p.

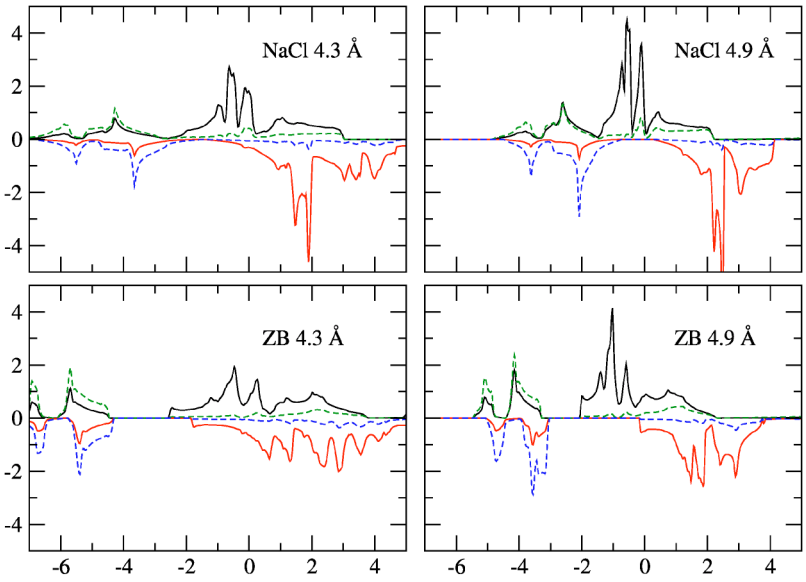

FIG. 5. (Color online) The DOS for CrN in both RS and ZB structures and with lattice constants of 4.3 and 4.9 Å, respectively.

nonbonding. They form weaker bonds with the other dangling bonds on the neighbors which are pointing away from the central transition metal atom.

The different bonding results in two significant differences in the band structure of NaCl and ZB structures, which explains the totally different behavior of the magnetism under volume expansion for the two structures. One difference is that there is a sharp gap between the *e* states and the bonding t_2-*p* states for the ZB structure. However for the NaCl structure, there is a small but nonzero DOS between the nonbonding t_{2g} and the e_g-*p* bonding states. Another significant difference between the two structures is the spin polarization. Near the equilibrium volume, the NaCl structure possesses a stronger spin polarization than the ZB structure. For instance, the splitting between the $t_{2g\uparrow}$ and $t_{2g\downarrow}$ in MnN at 4.3 Å is about 1.9 eV while in ZB, the splitting of the $e_\uparrow$ and $e_\downarrow$ is about 1.1 eV. The DOS shows that the noncoupling bands, *e* in ZB and t_{2g} in NaCl, are narrower and sharper in the NaCl structure, indicating that their interaction with the surrounding nitrogen atoms is weaker. Also, the peaks just below the Fermi level in ZB have actually a more mixed t_2 and *e* character while in RS they are more purely of t_{2g} character. The slightly stronger interaction for *e* states in ZB structure causes some delocalization of the *e* electrons and therefore results in a smaller spin polarization in comparison with the NaCl structure. Similar features are also found for CrN (see Fig. 5) and VN.

Figure 6 shows the PDOS of AFM CrN and MnN in the NaCl structure. The PDOS of one sublattice with fixed spin orientation is very similar to the FM total PDOS summed for both spins. Of course, the PDOS for spin-up and spin-down are equal because majority spin on one sublattice becomes minority on the other one. The major difference is that the gaps in both the majority and minority spins of the FM DOS are now filled with the states of the same spin on the other sublattice. These states filling the "gap" are primarily of t_{2g} character in the RS structure because those are the nonbonding states near the Fermi level.

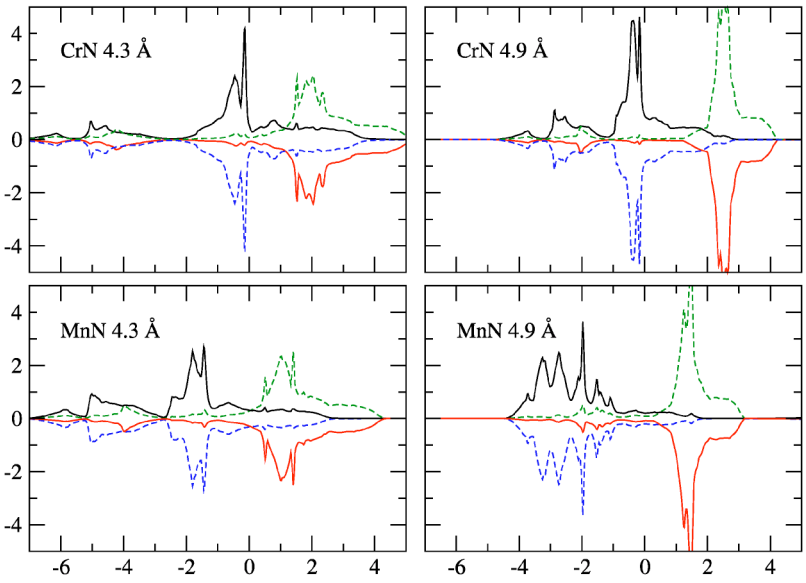

FIG. 6. (Color online) The DOS for MnN and CrN in AFM state and in RS structure and with lattice constants of 4.3 and 4.9 Å, respectively.

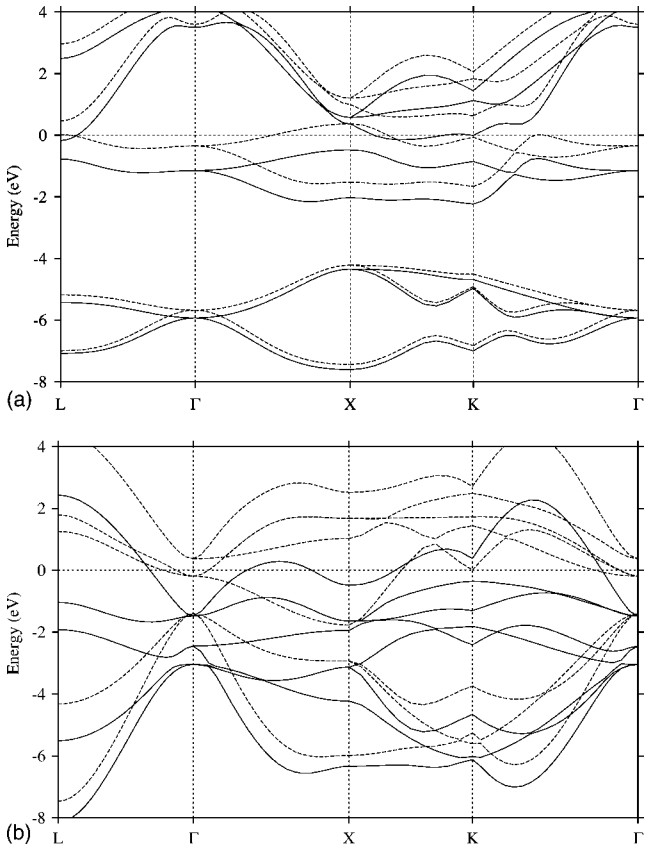

FIG. 7. Band structure of MnN in the FM state in both ZB (top) and RS (bottom) structures at the same lattice constant of 4.3 Å.

The band structures are shown for MnN in ZB and RS structures with a lattice constant of 4.3 Å in Fig. 7. One obvious difference in this figure is that in ZB, one has a separated set of three bands (of each spin) between −9 and −5.5 eV below the Fermi level. These bands are mostly N *p* in character or N *p* bonding with Mn *d* and Mn *sp* bands. One overall feature worth noting is that clearly the center of gravity of the occupied bands lies lower in ZB than in RS because of this separated band. This contributes to the stability of ZB relative to RS at this lattice constant. Although we noticed above that the Mn *d* to N sp^3 bonds are expected to be weaker in ZB than the Mn *d* e_g pure σ bonds to N *p* and N *s* we should keep into account that the Mn *s* electrons in tetrahedral environment may be thought of as forming Mn sp^3 hybrids which point directly toward the N sp^3 hybrids and contribute to these bands. Thus Mn 4*p* states may play a more signficant role in these bonding bands.

In RS, one may notice that at the Γ point, several eigenvalues occur very close to each other. This is because in the O_h symmetry *p* orbitals have different symmetry t_{1u} from *d* orbitals t_{2g} and so do not interact. The bands are in order of increasing energy $t_{1u\uparrow}$ purely N *p* like, $t_{2g\uparrow}$ purely Mn *d*, N *p* $t_{1u\downarrow}$, Mn *d* $e_{g\uparrow}$, Fermi level, Mn *d* $t_{2g\downarrow}$, Mn *d* $e_{g\downarrow}$, Mn *s* $a_{1\uparrow}$, Mn *s* $a_{1\downarrow}$. Of course, this pure symmetry classification only occurs at the Γ point. At other points, strong mixing of the bands occurs and one can no longer distinguish the bands as N *p*-like or Mn *d*-like. The mixed character of the bands is more clearly seen in the PDOS figures. However, the fact that the bands are not allowed to interact at Γ in RS whereas they are allowed in ZB leads to much stronger dispersion of some of the bands in RS. Several bands of both spin directions are seen to cross the Fermi level. Thus one may expect a complex Fermi surface. Furthermore it will be very different in ZB and in RS because the bands at the Fermi level are quite different. A detailed study of the Fermi surfaces is not carried out here because there are no experimental data to compare to.

TABLE II. Critical lattice constant a_{cr} in angstroms, magnetic moment μ in μ_B, minority band gap $E_g^{\downarrow}$ and spin-flip gap E_g^{sp} in electron volts, and majority DOS $N_{\uparrow}(E_F)$ at the Fermi level in states/eV/cell at $a=5$ Å.

	a_{cr}	μ	$E_g^{\downarrow}$	E_g^{sp}	$N_{\uparrow}(E_F)$
MnN	4.95	4	2.77	0.34	0.46
CrN	4.95	3	3.23	0.43	0.69
VN	4.95	2	3.51	0.44	0
FeN			−1.2	−0.52	0.67

C. Lattice expansion and half-metallicity

While the lattice is expanded, the coupling of the nitrogen *p* orbitals and the t_2 (in ZB) or e_g (in NaCl) becomes weaker. Therefore the crystal field spitting is reduced. This can be easily seen by checking the distances between the DOS peaks featuring e_g and t_2 states. In contrast, the spin splitting is evidently enhanced, especially for the ZB structure. At a lattice constant of 4.9 Å, the Fermi level is almost at the edge of the conduction bands of the minority spins, indicating that the system could become half-metallic at a large lattice expansion. Indeed, as revealed by a previous work, the half-metallicity is the results of both the increase of the minority band gap and the shift of the Fermi level away from the CBM, the two major effects of lattice expansion in a ZB structure. Although the lowest energy magnetic configuration in some of these compounds may be AFM, we study here the behavior of the FM state.

Table II lists the critical lattice constant for the appearance of half-metallicity, and the other major features for half-metallicity, the minority spin gap $E_g^{\downarrow}$, the spin-flip gap $E_g^{sp}=E_{CBM}^{\downarrow}-E_F$, and the majority spin density of states at the Fermi level $N_{\uparrow}(E_F)$ of all three nitrides as well as FeN at a lattice constants of 5.00 Å, close to the value of InN. The critical lattice constants are almost the same for the different nitrides. The energy difference between the Fermi level and the CBM of minority spin is a very important feature of half-metal materials and is also called the spin-flip gap. This gap is strongly dependent on the lattice constants. The values listed in Table II are calculated for a lattice expanded by about 20% from the equilibrium ZB lattice constant. The spin-flip gap is about 0.4 eV. This gap is only half of the value for the spin-flip gap of the other Cr and Mn pnictides under a lattice expansion of 10%. This indicates that the nitrides are bad candidates for half-metallicity.

We finally note that for FeN in the ZB structure we find only a very small or no magnetic moment and even at the

largest lattice constants considered it does not become half-metallic. The spin-flip and minority spin gaps are negative. On the other hand, the ZB structure is actually the equilibrium phase for FeN.[49]

IV. CONCLUSIONS

In this paper, we calculated the structure, the electronic and magnetic properties of MnN, CrN, and VN under various lattice expansions. We find that MnN has the ZB structure as the global energy minimum whereas CrN and VN have the NaCl structure as global energy minimum. Under volume expansion, all three nitrides have the ZB structure as lowest energy structure. They all obtain nonzero magnetic moments when carrying out spin polarized calculations. As far as the magnetic configuration is concerned we find that ZB MnN prefers the AFM-[001] ordering at a volume slightly larger than the equilibrium volume and prefers the AFM $[111]_1$ ordering at a larger volume. In contrast, CrN is FM in the ZB structure under lattice expansion. In the RS structure or CrN, we confirm the preference for AFM-[001] ordering in the absence of orthorhombic distortion that was obtained in previous calculations.[48] However, for larger lattice constants, we show that the AFM-$[110]_2$ ordering becomes preferred. This ordering is the experimental one but at the equilibrium lattice constant it is stabilized by an orthorhombic distortion. The magnetic interaction energies for MnN and CrN are quite large whereas for VN they are rather small. The NaCl structure shows a much larger spin polarization than the ZB structure near the equilibrium lattice constant. This is explained in terms of the differences in bonding which lead to narrower non or weakly bonding *d* bands in the RS than in the ZB structure.

Under lattice expansion, the spin polarization in ZB structure changes significantly. Only under very large lattice expansion, the system can become half-metallic.

Finally, we speculate about the possible relevance of some of our results to the observed room temperature ferromagnetism in TM-doped GaN. It is noteworthy that at the lattice constant of GaN 4.50 Å the nitrides considered here are already well above their equilibrium lattice constant for the ZB structure. One may thus speculate that if Mn or Cr in GaN would tend to phase seggregate into MnN or CrN precipitates, these could well be in the ZB phase to minimize the lattice mismatch with the surrounding host, being under a substantial strain. If so, our calculations predict that in the Cr case, these particles would be ferromagnetic and could indeed be partially responsible for the observed ferromagnetism. However, for the Mn case, the particles would be antiferromagnetic. Even so, they still indicate that permanent magnetic moments would form and the difference in energy between FM and AFM ordered states is small. In an external magnetic field it might be possible that these nanoparticles become ferromagnetic and contribute to the observed hysteresis. In any case, it would be useful to search for the occurence of such ZB, MnN, or CrN nanoscale particles in doped GaN systems.

ACKNOWLEDGMENTS

This work was supported by the Office of Naval Research under Grant No. N00014-02-0880 and the National Science Foundation under Grant No. ECS-0223634. Most of the calculations are performed on the Bewolf AMD cluster at the Ohio Supercomputing Center and supported under Project No. PDS0145.

[1] L. M. Corliss, N. Elliott, and J. M. Hastings, Phys. Rev. **117**, 929 (1960).
[2] J. D. Browne, R. R. Liddell, R. Street, and T. Mills, Phys. Status Solidi A **1**, 715 (1970) [CAS].
[3] P. Subramanya Herle *et al.*, J. Solid State Chem. **134**, 120 (1997).
[4] R. M. Ibberson and R. Cywinski, Physica B **181**, 329 (1992).
[5] A. Filippetti and N. A. Hill, Phys. Rev. Lett. **85**, 5166 (2000).
[6] G. Kreiner and H. Jacobs, J. Alloys Compd. **183**, 345 (1992).
[7] A. Leineweber, R. Niewa, H. Jacobs, and W. Kockelmann, J. Mater. Chem. **10**, 2827 (2000).
[8] Walter R. L. Lambrecht, Margarita Prikhodko, and M. S. Miao, Phys. Rev. B **68**, 174411 (2003).
[9] B. R. Sahu and L. Kleinman, Phys. Rev. B **68**, 113101 (2003).
[10] H. Akinaga, T. Manago, and M. Shirai, Jpn. J. Appl. Phys., Part 2 **39**, L1118 (2000).
[11] J. H. Zhao, F. Matsukura, K. Takamura, E. Abe, D. Chiba, and H. Ohno, Appl. Phys. Lett. **79**, 2776 (2001).
[12] K. Ono, J. Okabayashi, M. Mizuguchi, M. Oshima, A. Fujimori, and H. Akinaga, J. Appl. Phys. **91**, 8088 (2002).
[13] P. Ravindran, A. Delin, P. James, B. Johansson, J. M. Wills, R. Ahuja, and O. Eriksson, Phys. Rev. B **59**, 15680 (1999).
[14] S. Sanvito and N. A. Hill, Phys. Rev. B **62**, 15553 (2000).
[15] A. Continenza, S. Picozzi, W. T. Geng, and A. J. Freeman, Phys. Rev. B **64**, 085204 (2001).
[16] Y. J. Zhao, W. T. Geng, A. J. Freeman, and B. Delley, Phys. Rev. B **65**, 113202 (2002).
[17] Y.-Q. Xu, B.-G. Liu, and D. G. Pettifor, Phys. Rev. B **66**, 184435 (2002).
[18] I. Galanakis, P. H. Dederichs, and N. Papanikolaou, Phys. Rev. B **66**, 134428 (2002).
[19] B.-G. Liu, Phys. Rev. B **67**, 172411 (2003).
[20] W.-H. Xie, Y.-Q. Xu, B.-G. Liu, and D. G. Pettifor, Phys. Rev. Lett. **91**, 037204 (2003).
[21] I. Galanakis and P. Mavropoulos, Phys. Rev. B **67**, 104417 (2003).
[22] J. E. Pask, L. H. Yang, C. Y. Fong, W. E. Pickett, and S. Dag, Phys. Rev. B **67**, 224420 (2003).
[23] B. Sanyal, L. Bergqvist, and O. Eriksson, Phys. Rev. B **68**, 054417 (2003).
[24] W.-H. Xie, B.-G. Liu, and D. G. Pettifor, Phys. Rev. B **68**, 134407 (2003).
[25] D. D. Awschalom and J. M. Kikkawa, Phys. Today **52** (6), 33 (1999).
[26] S. A. Wolf, D. D. Awschalom, R. A. Buhrman, J. M. Daughton,

S. von Molnár, M. L. Roukes, A. Y. Chtchelkanova, and D. M. Treger, Science **294**, 1488 (2001).
[27] I. S. Osborne, Science **294**, 1483 (2001).
[28] W. E. Pickett and J. S. Moodera, Phys. Today **54**(5), 39 (2001).
[29] M. S. Miao and Walter R. L. Lambrecht, Phys. Rev. B **71**, 064407 (2005).
[30] M. L. Reed, N. A. El-Masry, H. H. Stadelmaier, M. K. Ritums, M. J. Reed, C. A. Parker, J. C. Roberts, and S. M. Bedair, Appl. Phys. Lett. **79**, 3473 (2001).
[31] S. E. Park, H.-J. Lee, Y. C. Cho, S.-Y. Jeong, C. R. Cho, and S. Cho, Appl. Phys. Lett. **80**, 4187 (2002).
[32] T. Dietl, H. Ohno, F. Matsukura, J. Cibert, and J. Ferrand, Science **287**, 1019 (2000).
[33] M. van Schilfgaarde and O. N. Mryasov, Phys. Rev. B **63**, 233205 (2001).
[34] K. Ando, Appl. Phys. Lett. **82**, 100 (2003).
[35] T. Graf, M. Gjukic, M. S. Brandt, M. Stuzmann, and O. Ambacher, Appl. Phys. Lett. **81**, 5159 (2002).
[36] N. Theodoropoulou, A. F. Hebard, M. E. Overberg, C. R. Abernathy, S. J. Pearton, S. N. G. Chu, and R. G. Wilson, Appl. Phys. Lett. **78**, 3475 (2001).
[37] S. S. A. Seo, M. W. Kim, Y. S. Lee, T. W. Noh, Y. D. Park, G. T. Thaler, M. E. Overberg, C. R. Abernathy, and S. J. Pearton, Appl. Phys. Lett. **82**, 4749 (2003).
[38] P. Hohenberg and W. Kohn, Phys. Rev. **136**, B864 (1964).
[39] W. Kohn and L. J. Sham, Phys. Rev. **140**, A1133 (1965).
[40] U. von Barth and L. Hedin, J. Phys. C **5**, 2064 (1972).
[41] M. Methfessel, M. van Schilfgaarde, and R. A. Casali, in *Electronic Structure and Physical Properties of Solids, The Uses of the LMTO Method*, edited by Hugues Dreyssé, Springer Lecture Notes, Workshop Mont Saint Odille, France, 1998 (Springer, Berlin, 2000), pp. 114–147.
[42] E. Bott, M. Methfessel, W. Krabs, and P. C. Schmidt, J. Math. Phys. **39**, 3393 (1998).
[43] C. Cheng, R. J. Needs, and V. Heine, J. Phys. C **21**, 1049 (1988).
[44] P. Subramanya Herle *et al.*, J. Solid State Chem. **134**, 120 (1997).
[45] D. A. Papaconstantopoulos, W. E. Pickett, B. M. Klein, and L. L. Boyer, Phys. Rev. B **31**, 752 (1985).
[46] H. Shimizu, M. Shirai, and N. Suzuki, J. Phys. Soc. Jpn. **66**, 3147 (1997); **67**, 922 (1998).
[47] A. Mavromaras, S. Matar, B. Siberchicot, and G. Demazeau, J. Magn. Magn. Mater. **134**, 34 (1994).
[48] A. Filippetti, W. E. Pickett, and B. M. Klein, Phys. Rev. B **59**, 7043 (1999).
[49] Pavel Lukashev and Walter Lambrecht (unpublished).